# Future Impact of Differential Inter-Basin Ocean Warming on Atlantic Hurricanes

Sang-Ki Lee[1], David B. Enfield[1] and Chunzai Wang[2]

[1] Cooperative Institute for Marine and Atmospheric Studies, University of Miami, Miami FL

[2] Atlantic Oceanographic and Meteorological Laboratory, NOAA, Miami FL

Submitted to Climate Dynamics

January 2010

Corresponding author address: Dr. Sang-Ki Lee, NOAA/AOML, 4301 Rickenbacker Causeway, Miami, FL 33149, USA. E-mail: Sang-Ki.Lee@noaa.gov.

## Abstract

Global climate model simulations forced by future greenhouse warming project that the tropical North Atlantic (TNA) warms at a slower rate than the tropical IndoPacific in the 21st century, consistent with their projections of the weakening Atlantic thermohaline circulation. Here, we use an atmospheric general circulation model to advance a consistent physical rationale that the suppressed warming of the TNA increases the vertical wind shear and moist static stability aloft, and thus decreases Atlantic hurricane activity in the 21st century. A carefully designed suite of model experiments illustrates that the preferential warming of the tropical IndoPacific induces a global average warming of the tropical troposphere, via a tropical teleconnection mechanism, and thus increases moist static stability and decreases convection over the suppressed warming region of the TNA. The anomalous diabatic-cooling, in turn, forces the formation of a stationary baroclinic Rossby wave northwest of the forcing region, consistent with the Gill's simple model of tropical atmospheric circulations, and thus induces a secular increase of the TNA vertical wind shear. A further analysis indicates that the net effect of future greenhouse warming on the MDR VWS is less than the observed multidecadal swing of the MDR VWS in the 20th century. Thus, it is likely that the Atlantic Multidecadal Oscillation will still play a decisive role over the greenhouse warming on the fate of Atlantic activity in the coming decades.

## 1. Introduction

Observations during the satellite era of 1965-2005 indicate that a 0.5$^{o}$C increase of North Atlantic Sea surface temperature (SST) in the main development region for hurricanes (MDR) is associated with about a 40% increase in Atlantic hurricane frequency (Saunders and Lea 2008). According to the externally forced model simulations for the 21st century used in the Intergovernmental Panel for Climate Change - 4th Assessment report (IPCC-AR4), the MDR SST may increase by about 2$^{o}$C or more between 2000 and 2100 due to anthropogenic global warming (AGW). This is alarming given that the MDR SST has never reached such an extremity since reliable, widespread instrumental measurements became available in the late 1800s. At issue is whether we are entering a new era of much elevated hurricane activity due to the rising global SST.

In the North Atlantic basin, the most critical environmental factors for hurricane intensification are the MDR vertical wind shear (VWS), which impedes the efficient development of organized convection to increasing heights as the storm intensity increases, and the MDR moist static instability of the troposphere (Emanuel, 1994). Thus, both the MDR VWS and moist static instability are useful and widely used proxies for overall Atlantic hurricane activity. In this study, the MDR convective precipitation rate (CPR) is used to represent the MDR moist static instability.

Figure 1 shows the seven-year running-averaged MDR (a) SST anomaly, (b) VWS (200mb minus 850mb) anomaly, and (c) CPR anomaly for the period of 1900-2100 obtained from the ensemble average of 21 IPCC-AR4 climate model simulations under the 20C3M (1900-1999) and SRESA1B (2000-2100) scenarios. The MDR SST increases monotonically by more than 2.5$^{o}$C between 1900 and 2100. The MDR VWS is characterized by an overall increase with relatively large amplitude of multidecadal variation in the 20th and 21st centuries, whereas the MDR moist static instability is significantly reduced between 1900 and 2100. Both the increased MDR VWS and decreased MDR moist static instability suggest that Atlantic cyclone activity could be reduced in the 21st century despite an increase in the MDR SST by 2.5$^{o}$C. Note that Wang and Lee (2008) also reported a similar upward trend in the observed MDR VWS during a relatively short period of 1949-2006.

The upward (downward) trend in MDR VWS (moist static instability) and the simultaneous increase in MDR SST are apparently inconsistent with recent research, which shows based on theory, observations and models that a warm tropical North Atlantic (TNA) SST significantly increases the MDR moist static instability and reduces the MDR VWS (Knight et al. 2006; Wang et al. 2006; Zhang and Delworth 2006). Therefore, it appears that using the observed correlation in the 20th century between the MDR SST and MDR VWS (or moist static instability) for projecting Atlantic hurricane activity of the 21st century could be misleading.

A newly emerging hypothesis provides us with some insights as to why this may be the case (Latif et al. 2007; Swanson 2008; Vecchi and Soden 2007b; Wang and Lee 2008). The main argument of the hypothesis is that Atlantic hurricanes do not respond to the absolute SST of MDR but to the SST difference between the MDR and the other tropical ocean basins (hereafter referred to as *differential inter-basin ocean warming hypothesis*). Therefore, it argues that an important and relevant question is if and how the MDR is warming at a different rate from the tropical IndoPacific under the AGW scenarios.

As shown in Figure 2, the IPCC-AR4 climate model simulations project that the TNA indeed warms at a slower rate than the tropical IndoPacific in the 21st century, which is consistent with their projections of the weakening Atlantic thermohaline circulation given an apparent coherent relation between the Atlantic thermohaline circulation and the TNA SST (Zhang and Delworth 2005; Timmermann et al. 2007; Zhang 2007; Chiang et al. 2008). It is also noticed that the equatorial Pacific (EQP), which is known to be an important region to remotely influence the MDR VWS (e.g. Goldenberg and Shapiro 1997; Latif et al. 2007), warms at a faster rate than the TNA and other tropical ocean regions, consistent with the IPCC-AR4 climate model projections of the weakening Pacific Walker circulation (Vecchi and Soden 2007c; DiNezio et al. 2009). Whatever the mechanism that causes the differential inter-basin ocean warming in the IPCC-AR4 climate model simulations, at issue is whether the suppressed warming of the TNA is the real cause of the secular increase (decrease) of the MDR VWS (moist static instability) in the 21st century. Given the observed correlation of El Niño with suppressed Atlantic hurricane activity in the 20th century (e.g. Goldenberg and Shapiro 1997; Latif et al. 2007), another interesting question is if the preferential warming of the EQP, in reference to the TNA and other tropical ocean regions, contributes to the secular increase (decrease) of the MDR VWS (moist static instability) in the 21st century.

To address these apparently important issues, here we explore the atmospheric dynamics that provide physical basis for the differential inter-basin ocean warming hypothesis by performing a set of climate model experiments using an atmospheric general circulation model. Toward the end, we attempt to explain the IPCC-AR4 projected secular increase (decrease) of the MDR VWS (moist static instability) in the

21st century by using the causal relationship of the inter-basin SST difference with the MDR VWS (moist static instability).

**2. Model Experiments**

The NCAR community atmospheric model version 3 (CAM3) is used as a primary tool for this study. The CAM3 is a global spectral model with a triangular spectral truncation of the spherical harmonics at zonal wave number 85 (T85) and with 26 hybrid sigma-pressure layers. The CAM3 is the atmospheric component of community climate system model version 3 (CCSM3), which is one of the climate models used in IPCC-AR4. Model experiments are performed by prescribing various composites of global SST and sea ice fraction, taken from the ensemble average of 11 IPCC-AR4 climate models simulations. The 11 IPCC-AR4 model simulations are selected because they show a clear upward trend of MDR VWS in the 21st century under SRESA1B scenario.

We have performed four sets of model experiments as summarized in Table 1. In the control experiment (EXP_CTRL), the global SSTs and sea ice fractions are prescribed with twelve monthly climatological values taken from the ensemble average of the 11 IPCC-AR4 climate simulations for the 2001-2020 periods. The $CO_2$ level is fixed to 380ppm, which is the averaged $CO_2$ level for 2001-2020 under SRESA1B scenario. Similarly, in the global ocean warming experiment (EXP_GLBW), the global SSTs and sea ice fractions are prescribed with twelve monthly climatological values taken from the ensemble average of the 11 IPCC-AR4 climate simulations for the 2081-2100 periods. The $CO_2$ level is fixed to 675ppm, which is the averaged $CO_2$ level for 2081-2100 under SRESA1B scenario. Figure 3a shows the SST difference between EXP_GLBW and

EXP_CTRL during the Atlantic hurricane season of June to November (JJASON). Comparing EXP_GLBW with EXP_CTRL, the MDR (85$^{o}$W-15$^{o}$W and 10$^{o}$N-20$^{o}$N) SST is warmer by 1.64$^{o}$C and the EQP (180$^{o}$W-85$^{o}$W and 5$^{o}$S-5$^{o}$N) SST is warmer by 2.20$^{o}$C, indicating a 0.56$^{o}$C per 80yr of differential warming rate between the two regions. In this sense, the global ocean warming experiment (EXP_GLBW) can be taken as a cooler TNA experiment (EXP_CTNA) or a warmer EQP experiment (EXP_WEQP).

The other two experiments are designed to understand the effects of the suppressed TNA warming and preferential EQP warming. In those two experiments, the global sea ice fractions are taken from the ensemble average of the 11 IPCC-AR4 climate simulations for 2081-2100 periods, and the $CO_2$ level is fixed to 675ppm following SRESA1B scenario. In the warmer TNA experiment (EXP_WTNA), SSTs in the suppressed warming region of the TNA (between the equator and 40$^{o}$N), where the SST difference of EXP_GLBW - EXP_CTRL is less than 1.75$^{o}$C, are increased in such a way that the MDR SST warming is equal to the EQP SST warming of 2.20$^{o}$C, whereas the SSTs outside of the North Atlantic Ocean are identical to those of EXP_GLBW. Similarly, in the cooler EQP experiment (EXP_CEQP), SSTs in the preferential warming region of the tropical Pacific (150$^{o}$E-eastern coast of South America and 10$^{o}$S-10$^{o}$N), where the SST difference of EXP_GLBW - EXP_CTRL is greater than 1.95$^{o}$C, are decreased in such a way that the EQP SST warming is equal to the MDR SST warming of 1.64$^{o}$C, whereas the SSTs outside of the tropical Pacific are identical to those of EXP_GLBW. The margins between the modified and unmodified parts of the SST field are smoothed. See Figure 3 and Table 1 for more details.

In each model experiment, the model is integrated for 25 years. The first 5 years of model output are discarded to exclude any possible transient spinup effects. The remaining 20 years of model output are averaged to suppress internal atmospheric variability. To isolate the effects of differential inter-basin ocean warming associated with AGW, the differences between EXP_GLBW and EXP_CTRL, between EXP_WTNA and EXP_GLBW, and between EXP_CEQP and EXP_GLBW are described and compared with the corresponding ensemble average of the 11 IPCC-AR4 climate simulations in the next section.

It is important to keep in mind that EXP_WTNA - EXP_GLBW represents a warmer minus cooler TNA, while EXP_CEQP - EXP_GLBW represents a cooler minus warmer EQP. In the case of EXP_GLBW - EXP_CTRL, many forcing factors are represented including (1) global ocean warming, (2) increased greenhouse gas, (3) suppressed warming of the TNA in reference to the tropical IndoPacific warming, and (4) preferential warming of the EQP in reference to warming in the TNA and other tropical oceans. In the next section, it will be shown and demonstrated that (3) is the only major factor to influence the MDR VWS and moist static instability.

**3. Results**

Figure 4a shows the VWS difference between 2080-2100 and 2000-2020 periods in JJASON computed from the ensemble average of the 11 IPCC-AR4 climate simulations under SRESA1B scenario, whereas Figure 4b and 4c show the VWS difference in JJASON between EXP_GLBW and EXP_CTRL, and between EXP_WTNA and EXP_GLBW, respectively. The composite difference in IPCC-AR4 model simulations

(Figure 4a) is characterized by an increase in the MDR VWS, particularly over the Caribbean Sea, with averaged amplitude of about 1.6 $ms^{-1}$ in the MDR box. The global ocean warming minus control run (Figure 4b) is also characterized by an increased MDR VWS, which is focalized over the same region (i.e. Caribbean Sea) as in the IPCC-AR4 composite difference (Figure 4a) with comparable amplitude. In this case, however, the MDR box-averaged VWS increases only by 0.6 $ms^{-1}$ because the positive VWS change is limited only over the Caribbean Sea.

In the warmer TNA minus global ocean warming run (Figure 4c), the MDR VWS over the Caribbean Sea is substantially weakened as expected from the earlier studies (Knight et al. 2006; Wang et al. 2006; Zhang and Delworth 2006) with about -1.7 $ms^{-1}$ averaged in the MDR box. This result clearly indicates that the MDR VWS increase in EXP_GLBW - EXP_CTRL can be negated or even reversed to foster more intense tropical storms in the North Atlantic basin if the warming rate of the MDR in the 21st century becomes as large as that of the EQP. The apparent similarity in the spatial pattern and amplitude of the MDR VWS changes between EXP_GLBW - EXP_CTRL (Figure 4b) and EXP_WTNA - EXP_GLBW (Figure 4c), strongly suggests that the main driver for the MDR VWS increase in EXP_GLBW - EXP_CTRL is the suppressed warming of the TNA in reference to the tropical IndoPacific (i.e. differential inter-basin ocean warming), and thus explains why a secular increase of MDR SST in the IPCC-AR4 model simulations does not necessarily result in a secular decrease in MDR VWS. We will come back to this point in the later part of this section where we present a consistent physical rationale that supports the differential inter-basin ocean warming hypothesis.

In the case of the cooler EQP minus global ocean warming run (EXP_CEQP – EXP_GBLW), the MDR VWS is reduced by more than -0.5 $ms^{-1}$ over the Caribbean Sea, but a slight increase in the central and eastern TNA nearly cancels out the net MDR VWS change (not shown). This means that the preferential warming of the EQP over the TNA and other tropical ocean regions is not an important feature that determines Atlantic cyclone activity of the 21st century. This result is surprising because a warming of the EQP associated with El Niño phenomenon is known to suppress Atlantic cyclone activity by increasing the MDR VWS (e.g. Goldenberg and Shapiro 1997; Latif et al. 2007). One logical explanation is that the preferential warming of the EQP (0.56$^{o}$C in this case) is not large enough to trigger a robust teleconnection to the North Atlantic Basin. Another possibility is that tropical atmospheric response to quasi-permanent warming of the EQP is much weaker than the tropical atmospheric response to transient EQP warming. Further studies are needed to clarify why the preferential warming of the EQP has little impact on the MDR VWS in the IPCC-AR4 climate model simulations.

To further understand the atmospheric dynamics associated with the MDR VWS changes shown in Figure 4, we now examine the horizontal gradient of geopotential thickness between the upper and lower troposphere, which is dynamically related to VWS via the thermal wind relationship. Figure 5a shows the geopotential thickness and VWS (200mb minus 850mb) vector differences in JJASON between 2080-2100 and 2000-2020 periods computed from the ensemble average of the 11 IPCC-AR4 climate simulations under SRESA1B scenario, whereas Figure 5b and c show the geopotential thickness and VWS vector differences in JJASON between EXP_GLBW and EXP_CTRL, and between EXP_WTNA and EXP_GLBW, respectively.

The composite difference of the IPCC-AR4 climate model simulations (Figure 5a) is clearly characterized by a region of minimal thickness and cyclonic vertical shear straddling the eastern North Pacific, Central American cordillera and the Gulf of Mexico. The global ocean warming minus control run (Figure 5b) also shows a similar pattern of the geopotential thickness and VWS vector differences, although in this case the Atlantic side of the cyclonic gyre is somewhat separated from the Pacific side by the Sierra Madre and Rocky mountains and much stronger than the Pacific side. The mean atmospheric circulation in boreal summer over the TNA features the easterly trade winds in the lower troposphere and the westerly winds in the upper troposphere. Thus, the wind patterns associated with the baroclinic cyclone strengthen both the lower-tropospheric easterly winds and the upper-tropospheric westerly winds over the Caribbean Sea, resulting in an increase of the MDR VWS.

In the case of the warmer TNA minus global ocean warming run (Figure 5c), on the other hand, an intense baroclinic anticyclone is formed in a broad region extending from the eastern North Pacific to the western TNA. The wind patterns associated with the baroclinic anticyclone decrease the MDR VWS. The baroclinic atmospheric response in this case is largely consistent with the Gill’s solution to a diabatic-heating in the TNA associated with the prescribed SST pattern (Figure 3b), and thus can be referred to as a heat-induced stationary baroclinic Rossby wave (Gill, 1980). It is immediately noticed that the baroclinic cyclone in EXP_GLBW - EXP_CTRL (Figure 5b) is almost a mirror image to the baroclinic anticyclone in EXP_WTNA - EXP_GLBW (Figure 5c), and thus consistent with the Gill’s solution to a diabatic-*cooling* in the TNA. However, note that the prescribed MDR SST is warmer in EXP_GLBW than in EXP_CTRL by 1.64$^{o}$C.

Apparently, the positive MDR SST forcing in EXP_GLBW - EXP_CTRL is in contradiction with a diabatic-cooling in the TNA.

To explain this conundrum, we present the following physical rationale. Even though the TNA SST is warmer in EXP_GLBW than in EXP_CTRL, the overlying atmosphere is also warmed due to the global average tropospheric warming of the tropics, which is largely induced by the increased SSTs in the tropical IndoPacific. Therefore, in this sense, the suppressed warming of the TNA increases the moist static stability and decreases the convection aloft, and thus evokes a Gill response consistent with local diabatic-cooling. As shown in Figure 6, the MDR moist static instability changes, corresponding to Figure 5, clearly support this rationale.

A similar argument has been used to explain the observed global tropospheric warming in the tropics associated with the El Niño (e.g. Chiang and Sobel 2002). The physical background for this argument is that equatorial Kelvin waves tend to redistribute temperature anomalies originating at one particular longitude band over the global tropical strip, which is a very efficient mechanism for tropical teleconnections. Note that the physical rationale provided here is consistent Xie et al. (2010) who showed the importance of regional differences in SST warming for tropical convection.

In summary, our model experiments cleanly demonstrated that the main driver for the increased MDR VWS and decreased MDR moist static instability in the 21st century, projected by the IPCC-AR4 climate model simulations, is the formation of baroclinic cyclone to the northwest of the MDR, which is a Gill response to a diabatic-cooling associated with the suppressed warming of the TNA in reference to the tropical IndoPacific.

## 4. Discussions

We now have a consistent physical rationale for expecting a significant relationship of a differential inter-basin ocean warming with the MDR VWS and moist static instability. Naturally, the next question is how well this relationship explains the secular increase (decrease) of the MDR VWS (moist static instability) within the 21st century projected by the IPCC-AR4 climate model simulations.

Figure 7a shows the time series of reconstructed MDR VWS in JJASON for the period of 1900-2100 based on a multiple regression of the MDR VWS onto the MDR SST and tropical IndoPacific (equator-30$^{o}$N) SST from the ensemble average of the 21 IPCC-AR4 climate model simulations under 20C3M and SRESA1B scenarios. The MDR CPR is also reconstructed using the MDR SST and tropical IndoPacific SST as the predictors for a multiple regression as shown in Figure 7b.

A close inspection of Figure 1 and 7 suggests that the original time series and the least squares fits share similar long-term signals and overall trend throughout 1900-2100 periods. The least squares equations used for reconstructing MDR VWS and CPR are given by MDR VWS = -2.7×MDR SST + 3.0×Tropical Indo Pacific SST, and MDR CPR = 0.9×MDR SST - 1.0×Tropical Indo Pacific SST, respectively. These equations clearly confirm that a uniform warming of the MDR SST and Tropical Indo Pacific SST has little impact on the MDR VWS and moist static instability, which are the two most critical environmental factors for Atlantic hurricane activity, and that the inter-basin SST difference is the most important indicator and predictor of Atlantic hurricane activity for both the 20th and 21st centuries.

At the multidecadal or longer time scales, the observed MDR VWS during 1949-2006 periods changes by up to 4.0 $ms^{-1}$ (Wang et al. 2009), whereas the ensemble-average of IPCC-AR4 model simulations projects that the MDR VWS increases by about 1.0 $ms^{-1}$ in the 21st century (Figure 1b). Therefore, the net effect of AGW on the MDR VWS is less than the observed multidecadal swing in the 20th century associated with the Atlantic Multidecadal Oscillation (AMO). Apparently, the IPCC-AR4 model simulations underestimate the multidecadal swing of the observed MDR VWS in the 20th century. This is partly because the internally generated multidecadal signals are canceled out after applying the ensemble mean (Knight 2009; Ting et al. 2009). Thus, it is likely that the multidecadal signals in the ensemble-averaged MDR VWS (Figure 1b) are primarily caused by fluctuations of aerosols in the 20th century (Knight 2009).

An important and practical question is why the tropical IndoPacific warms faster than the TNA in the IPCC-AR4 climate model simulations for the 21st century. Given the existing evidence from research that the cold AMO phase occurs in concert with decreases in the Atlantic thermohaline circulation (e.g. Delworth and Mann 2000), the suppressed warming of the TNA, in reference to the tropical IndoPacific, is consistent with the IPCC-AR4 projection of a significantly weakened Atlantic Meridional Overturning Circulation in the 21st century. Apart from the potential contributions of the weakening Atlantic thermohaline circulation, recent studies by Leloup and Clement (2009), and Xie et al. (2010) provide an alternative explanation for the suppressed warming of the TNA. Their main argument is that a uniform increase of SST may result in a greater evaporative cooling response in the region of high mean surface wind speed such as in the TNA because the mean surface wind speed serves as the efficiency of evaporative cooling response to external forcing. Further studies are warranted to clarify why the IPCC-AR4 climate models project a suppressed warming in the TNA and how reliable that projection is.

Finally, there remains another crucial question. Is the suppressed warming of the TNA in the IPCC-AR4 climate model simulations detectable from observed SST records of the 20th century? Unfortunately, we do not have a clear answer to this question because it is virtually impossible to cleanly separate the secular trend of observed MDR SST from the multidecadal signal of the AMO, which is the dominant mode of SST variability in the North Atlantic. For instance, during 1901-2008, the Hadley Center sea ice and sea surface temperature (HadISST) and extended reconstructed SST (ERSST3) data give 1.1 and 1.5$^{o}$C per 100 yrs of secular trends of MDR SST, respectively. During the same period, the secular trends of the tropical IndoPacific (equator-30$^{o}$N) SST in HadISST and ERSST3 are 1.0 and 1.4$^{o}$C per 100 yrs, respectively, indicating a preferential warming of the TNA. However, if a positive AMO phase of 1996-2008 is excluded, the secular trends of MDR SST in the HadISST and ERSST3 drastically drop to 0.8 and 1.2$^{o}$C per 100 yrs, respectively, whereas the secular trends of the tropical IndoPacific SST in HadISST and ERSST3 become 0.9 and 1.3$^{o}$C per 100 yrs, respectively, indicating a suppressed warming of the TNA. An important message here is that the AMO will still play a decisive role over the AGW on the fate of Atlantic activity in the coming decades (Enfield and Cid-Serrano 2009).

**Acknowledgments.** This work was supported by a grant from National Oceanic and Atmospheric Administration (NOAA) Climate Program Office. We thank three anonymous reviewers for their useful suggestions, which led to a significant improvement of the model experiment design. The findings and conclusions in this report are those of the authors and do not necessarily represent the views of the funding agency.

## References

Chiang JCH, Sobel AH (2002) Tropical tropospheric temperature variations caused by ENSO and their influence on the remote tropical climate. J Clim 15:2616-2631

Chiang JCH, Cheng W Bitz CM (2008) Fast teleconnections to the tropical Atlantic sector from Atlantic thermohaline adjustment. Geophys Res Lett 35:L07704. doi:10.1029/2008GL033292

Delworth TL, Mann ME (2000) Observed and simulated multidecadal variability in the Northern Hemisphere. Clim Dyn 16:661-676

Enfield DB, Cid-Serrano L (2009) Secular and multidecadal warmings in the North Atlantic and their relationships with major hurricane activity. Int J Clim 28. doi: 10.1002/joc.1881

DiNezio PN, Clement AC, Vecchi GA, Soden BJ, Kirtman BP, Lee S-K (2009) Climate response of the equatorial Pacific to global warming. J Clim 22:4873-4892

Gill AE (1980) Some simple solutions for heat-induced tropical circulation. Quart J Roy Meteor Soc 106:447-462

Goldenberg SB, Shapiro LJ (1996) Physical mechanisms for the association of El Niño and West African rainfall with Atlantic major hurricane activity. J Clim 9:1169-1187

Knight JR, Folland CK, Scaife AA (2006) Climate impacts of the Atlantic Multidecadal Oscillation. Geophys Res Lett 33:L17706. doi:10.1029/2006GL026242

Knight JR (2009) The Atlantic multidecadal oscillation inferred from the forced climate reponse in coupled general circlualation models. J Clim 22:1610-1625

Latif M, Keenlyside N, Bader J (2007) Tropical sea surface temperature, vertical wind shear, and hurricane development. Geophys Res Lett 34**:**L01710**.** doi:10.1029/2006GL027969

Leloup J, Clement A (2009) Why is there a minimum in projected warming in the tropical North Atlantic Ocean? Geophys Res Lett 36:L14802. doi:10.1029/2009GL038609

Saunders MA, Lea AS (2008) Large contribution of sea surface warming to recent increase in Atlantic hurricane activity. Nature 451:557-560

Swanson KL (2008) Nonlocality of Atlantic tropical cyclone intensities. Geochem Geophys Geosyst 9:Q04V01. doi:10.1029/2007GC001844

Timmermann A, Okumura Y, An SI, Clement A, Dong B, Guilyardi E, Hu A, Jungclaus JH, Renold M, Stocker TF, Stouffer RJ, Sutton R, Xie S-P, and Yin J (2007) The influence of a weakening of the Atlantic meridional overturning circulation on ENSO. J Clim 20:4899–4919

Ting M, Kushnir Y, Seager R, Li C (2009) Forced and internal twentieth-century SST trends in the North Atlantic. J Clim 22:1469–1481

Vecchi GA, Soden BJ (2007a) Increased tropical Atlantic wind shear in model projections of global warming. Geophys Res Lett 34:L08701. doi:10.1029/2006GL028905

Vecchi GA, Soden BJ (2007b) Effect of remote sea surface temperature change on tropical cyclone potential intensity. Nature 450:1066-1070. doi:10.1038/nature06423

Vecchi GA, Soden BJ (2007c) Global warming and the weakening of the tropical circulation. J Clim 20:4316–4340

Wang C, Enfield DB, Lee S-K, Landsea CW (2006) Influences of Atlantic warm pool on Western Hemisphere summer rainfall and Atlantic hurricanes. J Clim 19:3011-3028.

Wang C, Lee S-K (2008) Global warming and United States landfalling hurricanes. Geophys Res Lett 35:L02708. doi:10.1029/2007GL032396

Wang C, Lee S-K Enfield DB, (2009) Atlantic warm pool acting as a link between Atlantic multidecadal oscillation and Atlantic tropical cyclone activity. Geochem Geophys Geosyst 9:Q05V03. doi:10.1029/2007GC001809

Xie, S-P, Deser C, Vecchi GA, Ma J, Teng H, and Wittenberg AT (2010) Global warming pattern formation: Sea surface temperature and rainfall. J Clim In-press

Zhang R, and Delworth TL (2005) Simulated tropical response to a substantial weakening of the Atlantic thermohaline circulation. J Clim 18:1853-1860

Zhang R, Delworth TL (2006) Impact of Atlantic multidecadal oscillations on India/Sahel rainfall and Atlantic hurricanes. Geophys Res Lett 33:L17712. doi:10.1029/2006GL026267

Zhang R (2007) Anticorrelated multidecadal variations between surface and subsurface tropical North Atlantic. Geophys Res Lett 34:L12713. doi:10.1029/2007GL030225

**Table 1**. Global SST and sea-ice fraction prescribed in the four CAM3 experiments are obtained from the ensemble average of 11 IPCC-AR4 climate simulations for the 21st century under SRESA1B scenario for the periods described in this table. Also shown in this table are the EQP and MDR SST increases in each experiment in reference to the control experiment. CO2 level specified for the three experiments are also summarized in this table. See text for more detail.

| Experiments | EQP SST Increase | MDR SST Increase | Global SST | Sea Ice Fraction | $CO_2$ Level |
|---|---|---|---|---|---|
| EXP_CTRL | - | - | 2001 ~ 2020 | 2001 ~ 2020 | 380ppm |
| EXP_GLBW | 2.20 | 1.64 | 2081 ~ 2100 | 2081 ~ 2100 | 675ppm |
| EXP_WTNA | 2.20 | 2.20 | 2081 ~ 2100 | 2081 ~ 2100 | 675ppm |
| EXP_CEQP | 1.64 | 1.64 | 2081 ~ 2100 | 2081 ~ 2100 | 675ppm |

**Figure 1**. Seven-year running mean (a) SST anomaly, (b) VWS (200mb minus 850mb) anomaly and (c) CPR anomaly averaged in the MDR ($85^oW$-$15^oW$, $10^oN$-$20^oN$) for the period of 1900-2100 obtained from the ensemble average of 21 IPCC-AR4 climate model simulations under the 20C3M (1900-1999) and SRESA1B (2000-2100) scenarios. The period of 1900-1999 is used as the baseline for computing the anomalies. Gray lines represent 95% significance, which is computed based on a bootstrap technique.

**Figure 2**. Linear trend of SST (in unit of $^{o}$C per 100 years) in JJASON during 2000-2100 periods computed from the ensemble average of 21 IPCC-AR4 climate simulations under SRESA1B scenario.

**Figure 3**. SST difference (in unit of $^{o}$C) in JJASON for (a) EXP_GLBW - EXP_CTRL, (b) EXP_WTNA - EXP_GLBW and (c) EXP_CEQP - EXP_GLBW. The two box regions indicate the MDR for Atlantic hurricanes (85$^{o}$W-15$^{o}$W, 10$^{o}$N-20$^{o}$N) and the EQP (180$^{o}$W-85$^{o}$W and 5$^{o}$S-5$^{o}$N). Note that (b) EXP_WTNA – EXP_GLBW represents a warmer minus cooler TNA, while (c) EXP_CEQP - EXP_GLBW represents a cooler minus warmer EQP.

**Figure 4**. (a) VWS (200mb minus 850mb) difference in JJASON between 2080-2100 and 2000-2020 periods computed from the ensemble average of 11 IPCC-AR4 climate simulations under the SRESA1B scenario. The VWS difference in JJASON for (b) EXP_GLBW - EXP_CTRL and (c) EXP_WTNA - EXP_GLBW. White areas are mountain regions without 850mb data. VWS difference for EXP_CEQP - EXP_GLBW is not shown because it is small.

**Figure 5.** (a) Geopotential thickness and VWS vector (200mb minus 850mb) differences in JJASON between 2080-2100 and 2000-2020 periods computed from the ensemble average of 11 IPCC-AR4 climate simulations under SRESA1B scenario. Geopotential thickness and VWS vector differences in JJASON for (b) EXP_GLBW - EXP_CTRL and (c) EXP_WTNA - EXP_GLBW. White areas are mountain regions without 850mb data.

Dynamic responses of the atmosphere to AGW are most prominent over high-latitudes around 50 ~ 60$^{o}$N with a significant amplitude in zonally averaged components (not shown). Since the main interest is tropical atmospheric dynamics around the MDR, the zonal mean components of geopotential thickness difference are removed. Note that the zonal means are not removed in VWS difference. Geopotential thickness and VWS vector differences for EXP_CEQP - EXP_GLBW are not shown because they are small.

**Figure 6**. (a) CPR difference (in unit of mm day$^{-1}$) in JJASON between 2080-2100 and 2000-2020 periods computed from the ensemble average of the 11 IPCC-AR4 climate simulations under SRESA1B scenario. The CPR difference in JJASON for (b) EXP_GLBW - EXP_CTRL and (c) EXP_WTNA - EXP_GLBW. CPR difference for EXP_CEQP - EXP_GLBW is not shown because it is small.

**Figure 7**. Times series of reconstructed (a) MDR VWS and (b) CPR in JJASON for the period of 1900-2100 based on multiple regressions of the MDR VWS and CPR onto the MDR SST and tropical IndoPacific SST (equator-30$^{o}$N) from the ensemble average of 21 IPCC-AR4 climate model simulations under 20C3M and SRESA1B scenarios. Seven-year running mean is applied to all indices before applying the multiple regressions.

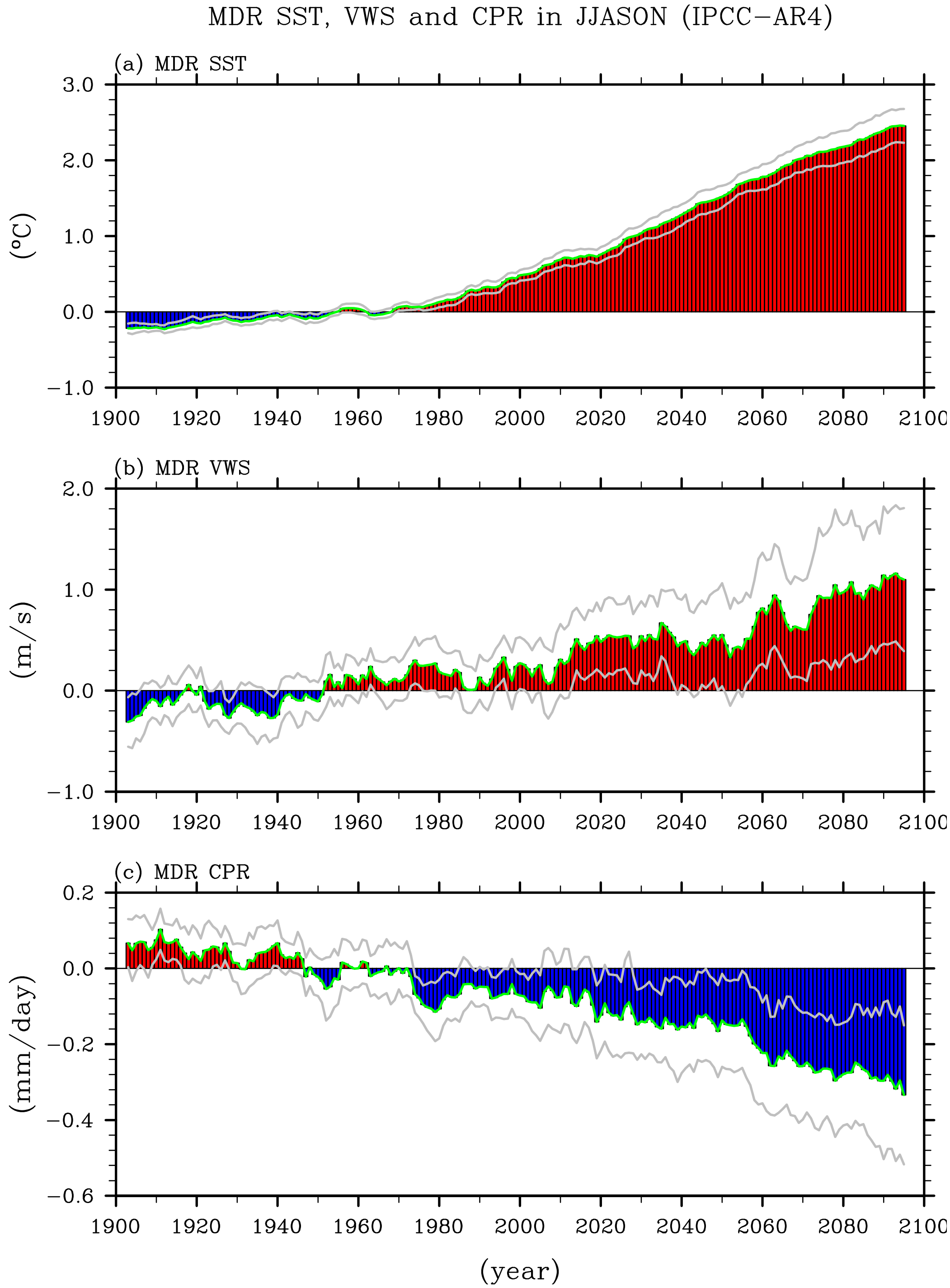
MDR SST, VWS and CPR in JJASON (IPCC−AR4)
(a) MDR SST
(°C)
3.0
2.0
1.0
0.0
−1.0
1900
1920
1940
1960
1980
2000
2020
2040
2060
2080
2100
(b) MDR VWS
(m/s)
2.0
1.0
0.0
−1.0
(c) MDR CPR
(mm/day)
0.2
0.0
−0.2
−0.4
−0.6
(year)

**Figure 1**.

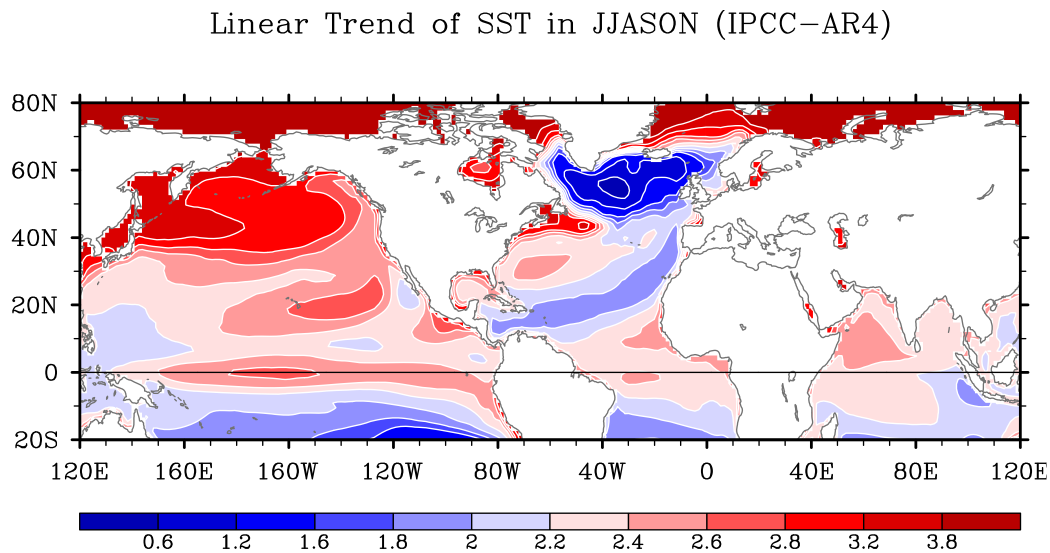
Linear Trend of SST in JJASON (IPCC−AR4)
80N
60N
40N
20N
0
20S
120E
160E
160W
120W
80W
40W
0
40E
80E
120E
0.6
1.2
1.6
1.8
2
2.2
2.4
2.6
2.8
3.2
3.8

**Figure 2**.

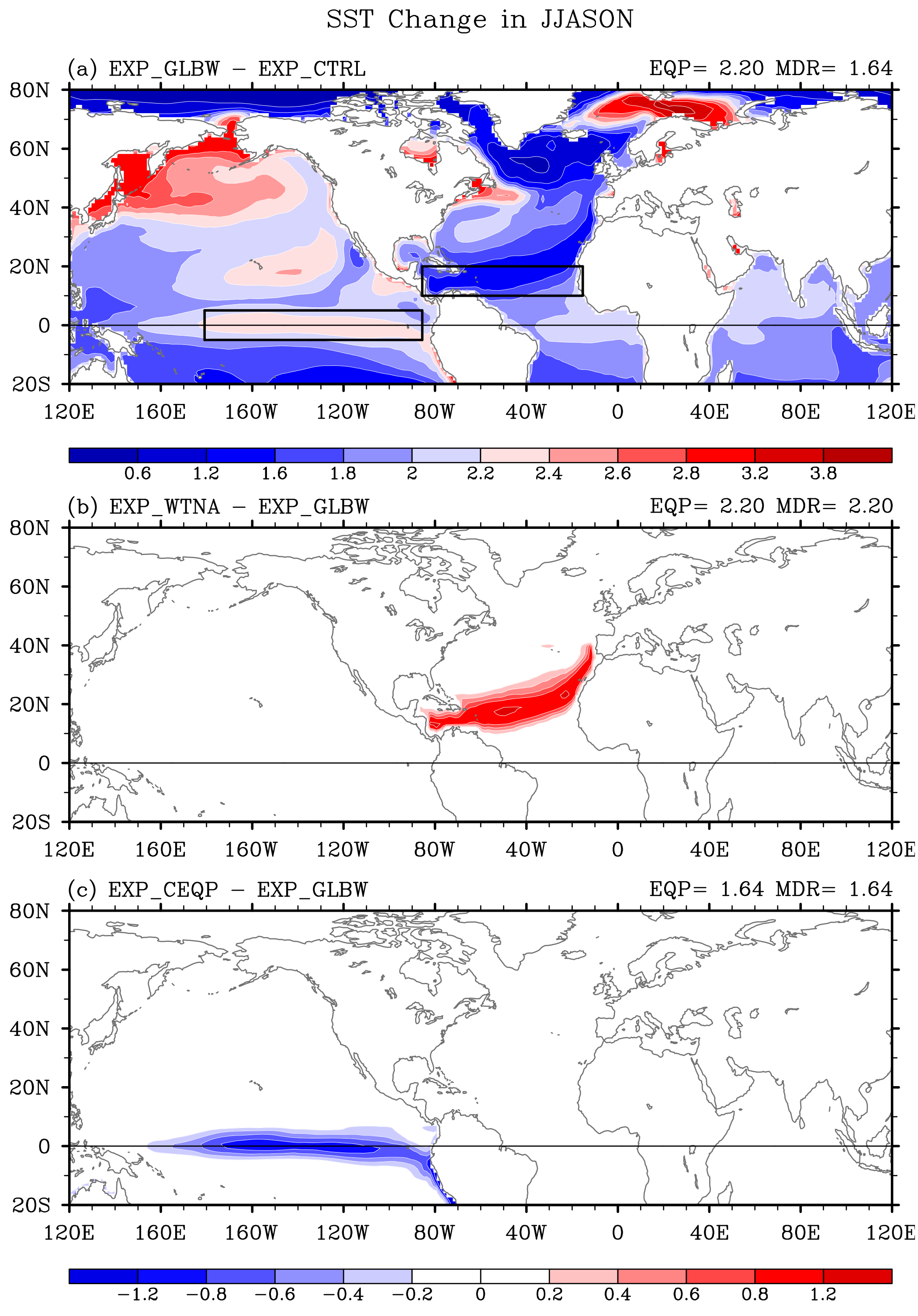
SST Change in JJASON
(a) EXP_GLBW − EXP_CTRL
EQP= 2.20 MDR= 1.64
80N
60N
40N
20N
0
20S
120E
160E
160W
120W
80W
40W
0
40E
80E
120E
0.6
1.2
1.6
1.8
2
2.2
2.4
2.6
2.8
3.2
3.8
(b) EXP_WTNA − EXP_GLBW
EQP= 2.20 MDR= 2.20
(c) EXP_CEQP − EXP_GLBW
EQP= 1.64 MDR= 1.64
−1.2
−0.8
−0.6
−0.4
−0.2
0
0.2
0.4
0.6
0.8
1.2

**Figure 3.**

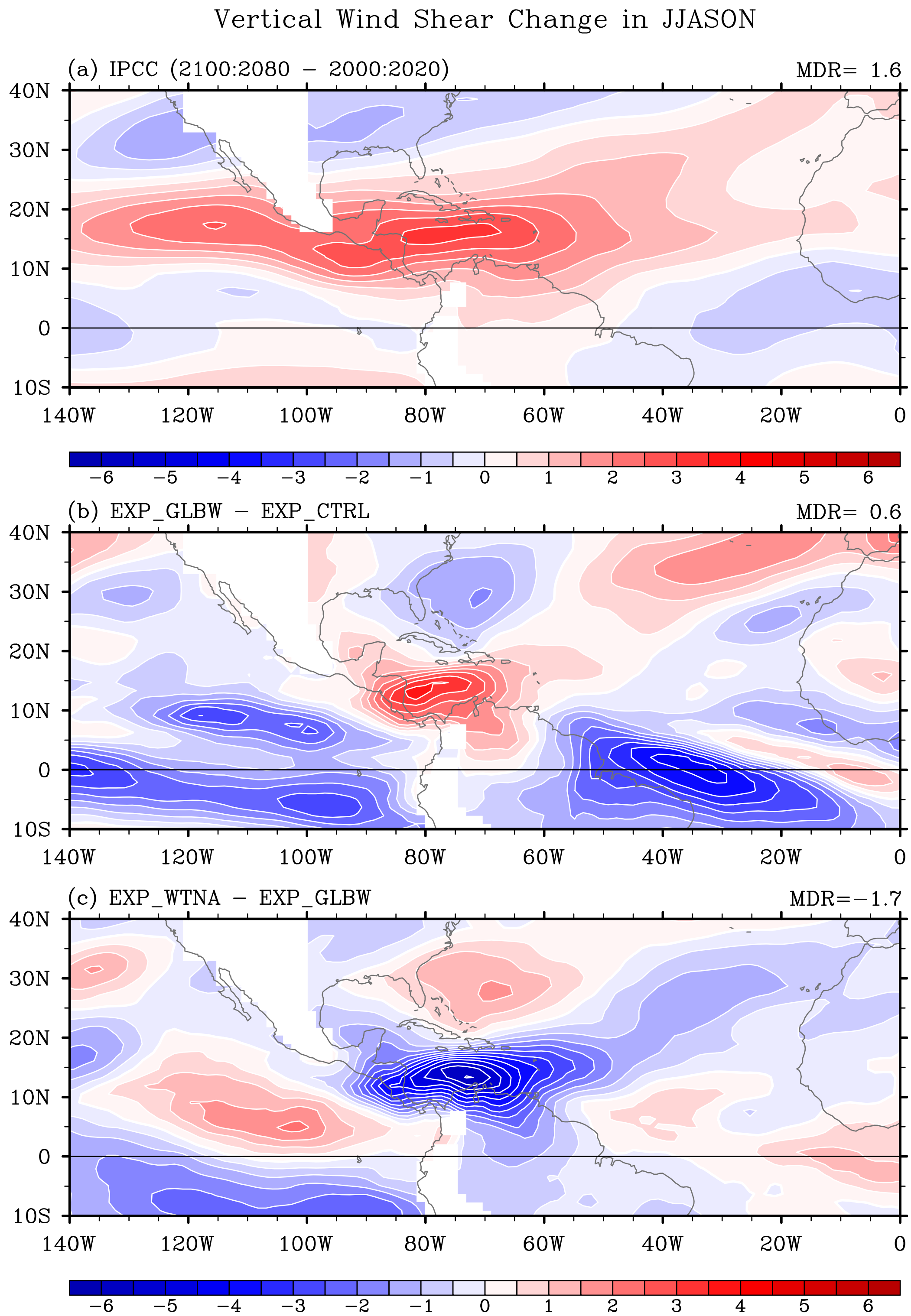

Vertical Wind Shear Change in JJASON
(a) IPCC (2100:2080 – 2000:2020)
MDR= 1.6
40N
30N
20N
10N
0
10S
140W
120W
100W
80W
60W
40W
20W
0
−6
−5
−4
−3
−2
−1
0
1
2
3
4
5
6
(b) EXP_GLBW – EXP_CTRL
MDR= 0.6
(c) EXP_WTNA – EXP_GLBW
MDR=−1.7


**Figure 4**.

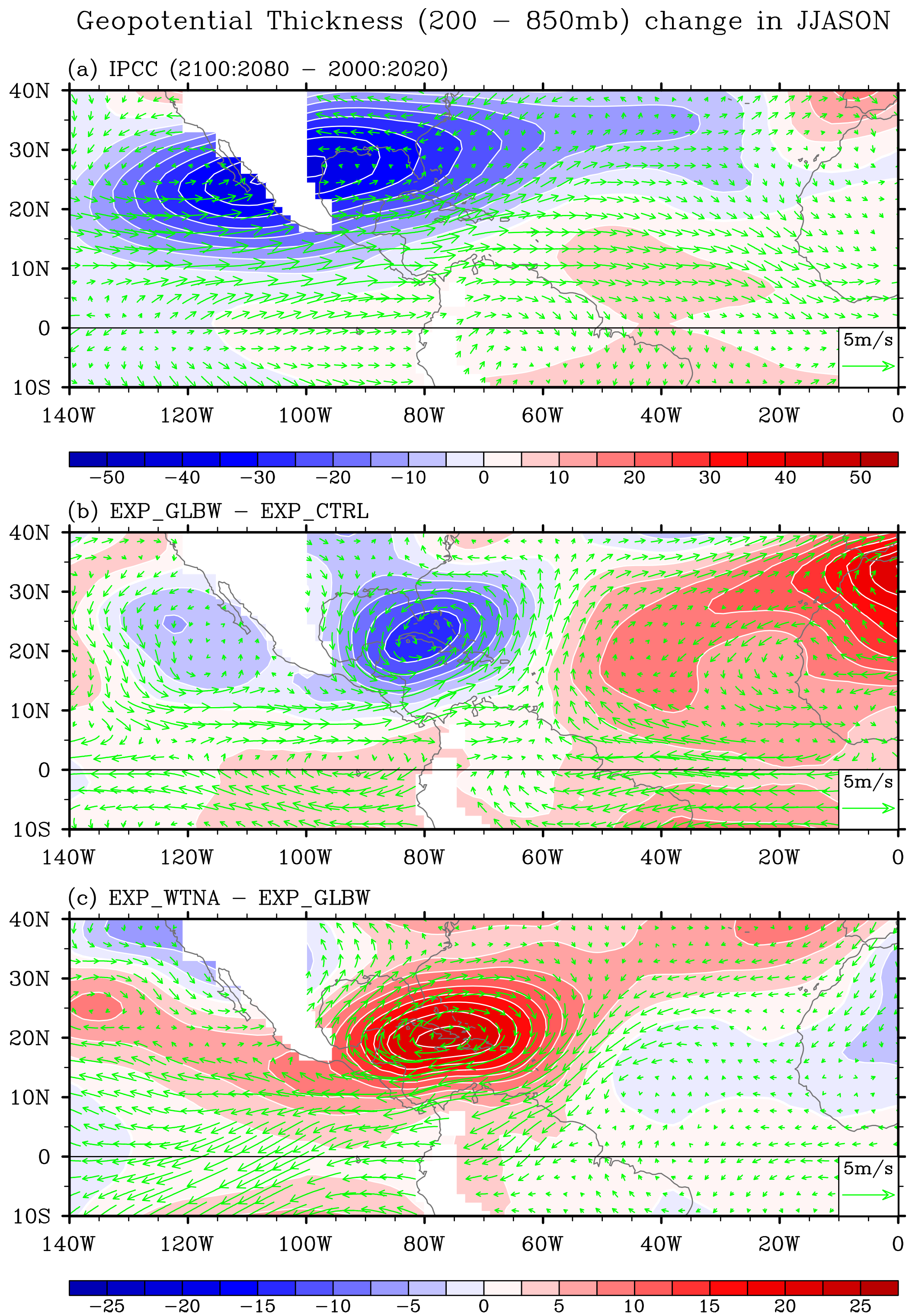

Geopotential Thickness (200 – 850mb) change in JJASON
(a) IPCC (2100:2080 – 2000:2020)
40N
30N
20N
10N
0
10S
140W
120W
100W
80W
60W
40W
20W
0
5m/s
−50
−40
−30
−20
−10
0
10
20
30
40
50
(b) EXP_GLBW – EXP_CTRL
(c) EXP_WTNA – EXP_GLBW
−25
−20
−15
−10
−5
0
5
10
15
20
25


**Figure 5**.

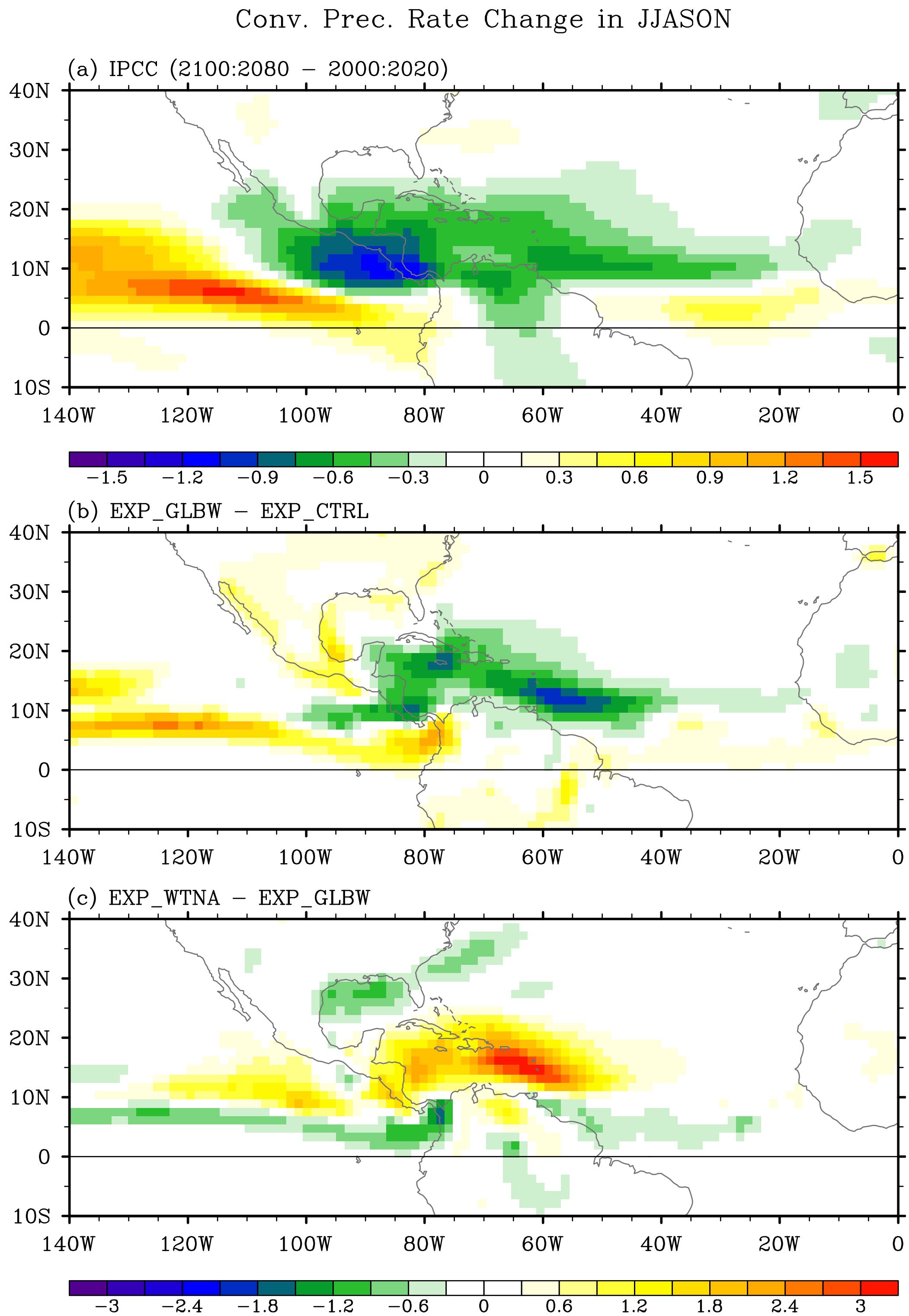
Conv. Prec. Rate Change in JJASON
(a) IPCC (2100:2080 – 2000:2020)
40N
30N
20N
10N
0
10S
140W
120W
100W
80W
60W
40W
20W
0
−1.5
−1.2
−0.9
−0.6
−0.3
0
0.3
0.6
0.9
1.2
1.5
(b) EXP_GLBW – EXP_CTRL
(c) EXP_WTNA – EXP_GLBW
−3
−2.4
−1.8
−1.2
−0.6
0
0.6
1.2
1.8
2.4
3

**Figure 6.**

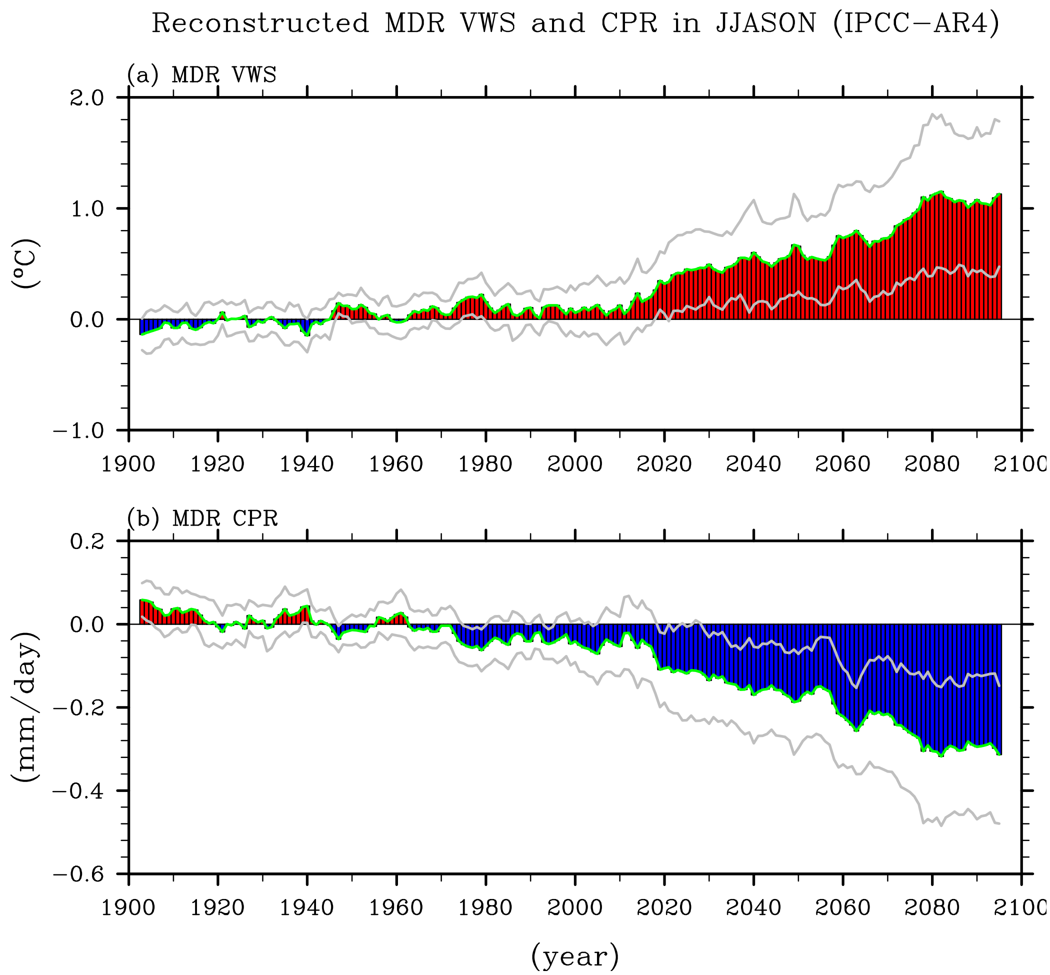
Reconstructed MDR VWS and CPR in JJASON (IPCC−AR4)
(a) MDR VWS
2.0
1.0
0.0
−1.0
(ºC)
1900
1920
1940
1960
1980
2000
2020
2040
2060
2080
2100
(b) MDR CPR
0.2
0.0
−0.2
−0.4
−0.6
(mm/day)
(year)

**Figure 7**.